International Journal of Hydrogen Energy 210 (2026) 153629

Contents lists available at ScienceDirect

International Journal of Hydrogen Energy

journal homepage: www.elsevier.com/locate/he

Topology-aware hydrogen injection planning in natural gas pipeline networks: A case study for California

Zemin Eitan Liu [a,*], Zhenlin Chen [b], Wennan Long [a,e], Liang Jing [c], Diego Moya [c], Bo Ren [d], Farah Ramadan [e], Abdulelah S. Alshehri [f], Mohammad S. Masnadi [a,*]

[a] Chemical and Petroleum Engineering Department, University of Pittsburgh, Pittsburgh, 15213, PA, USA
[b] Energy Science Engineering, Stanford University, Stanford, 94305, CA, USA
[c] Energy Sustainability Analysis Team, Technology Strategy & Planning Department, Saudi Aramco, Dhahran, 34465, Saudi Arabia
[d] Global Technology Analysis Team, Aramco Research Center-Houston, Aramco Americas, Houston, 77084, TX, USA
[e] Global Technology Analysis Team, Aramco Research Center -Novi, Aramco Americas, Novi, 48377, MI, USA
[f] Department of Chemical Engineering, College of Engineering, King Saud University, Riyadh, 11421, Saudi Arabia

ARTICLE INFO

Keywords:
Hydrogen blending
Natural gas pipeline networks
Topology-aware energy modeling
Hydrogen injection optimization
Clean energy transition
California case study

ABSTRACT

Hydrogen blending into natural gas networks is a candidate pathway for decarbonizing power generation while utilizing existing infrastructure. Yet, the effectiveness of such a decarbonization strategy is highly sensitive to the geospatial topology of transmission networks and the distribution of hydrogen injection points. This study presents a topology-aware planning and pathway-tracing framework for constructing California's regional natural gas transport patterns and evaluating hydrogen injection strategies across three representative areas: the Bay Area, Los Angeles, and Bakersfield. The transmission network in each region is decomposed into a set of tree-like structures rooted at processing plants and terminating at power plants. Three coverage metrics, including pathway, plant, and flow, are defined to quantify hydrogen accessibility and diffusion, and show that coverage is a key determinant of both regional hydrogen penetration and heating-value uniformity. A multi-objective optimization and simulation model is also established to evaluate distributed, centralized, and optimization-based injection strategies. The results reveal clear trade-offs between hydrogen penetration and variance in gas heating-value. The findings highlight the topological sensitivity of hydrogen distribution, where facilities located near supply-tree roots exert broader influence but may entail higher transport costs and risks. Building on the framework, topology-sensitive and cost-aware planning strategies are proposed, including targeted siting of new facilities at the lowest common ancestors or cross-tree nodes to improve coverage and reduce heating-value disparities. The framework provides a scalable, generalizable tool for topology-aware simulation and policy-configurable optimization under real-world network constraints, supporting decision-making in clean-energy transitions.

1. Introduction

Hydrogen is widely recognized as a promising energy carrier towards a low-carbon economy. It can be produced from diverse low-carbon sources and deployed across diverse sectors, including seasonal energy storage, transportation, and heating and power for residential, commercial, and industrial users [1–3]. However, a key barrier to large-scale adoption lies in the development of infrastructure to support these applications. To circumvent the high costs of dedicated hydrogen networks, exploring the integration of hydrogen into existing natural gas pipeline systems has gained growing interest [4,5].

Leveraging existing natural gas infrastructure provides a cost-effective and scalable pathway for transporting and storing hydrogen [6,7]. Injecting hydrogen into natural gas pipelines could defer some investment in new transmission assets while enabling line-pack and geologic storage across extensive networks [8]. This approach may create early electrolysis markets by connecting to dispersed demand centers.

Hydrogen-natural gas blends reduce greenhouse gas emissions when hydrogen comes from renewable electricity (wind, solar, or hydro) [9]. This integration mirrors gas-electricity system coordination [10,11] and may improve flexibility in balancing energy supply and demand. In heating, power generation, and transportation, blended fuels can reduce SO_x, NO_x emissions [12,13]. Furthermore, hydrogen blending enables efficient long-distance delivery to remote locations via existing

* Corresponding authors.
E-mail addresses: eliuzm@163.com (Z.E. Liu), m.masnadi@pitt.edu (M.S. Masnadi).

https://doi.org/10.1016/j.ijhydene.2026.153629
Received 10 September 2025; Received in revised form 26 December 2025; Accepted 19 January 2026
Available online 22 January 2026

pipelines, with localized extraction near end-user sites providing a cost-effective alternative to high-pressure hydrogen pipelines.

Despite these advantages, hydrogen blending into natural gas networks poses several technical and operational challenges that must be carefully considered in both infrastructure planning and policy design. Hydrogen can cause pipeline steel embrittlement, weakening structural integrity over time [14,15]. Hydrogen's lower volumetric energy density (12.7 MJ/m^3 versus 39.8 MJ/m^3 for methane) also requires higher flow rates for equivalent energy delivery, increasing stress on pipeline capacity and flow management systems [16]. Moreover, most existing compressor stations are not optimized for hydrogen, which can reduce efficiency and raise operational costs [17]. Safety is another concern, as hydrogen's wide flammability range, low ignition energy, and high diffusivity elevate the risk of leakage and explosion [18]. These constraints indicate the need for rigorous technical standards and regulatory frameworks to ensure safe and cost-effective deployment.

The power generation sector represents a particularly compelling end-user for hydrogen injection into natural gas networks, accounting for the largest share (≈40%) of U.S. natural gas, ahead of the industrial, residential, commercial, and transportation sectors [19]. Integrating hydrogen into the power generation sector fuel stream offers a great opportunity to enhance sustainability and accelerate energy system decarbonization. The geographic distribution of power generation facilities also provides a scalable platform for hydrogen deployment that extends to other applications.

Hydrogen produced from renewable electricity serves as an effective energy storage medium, allowing power systems to absorb excess generation and return it later as dispatchable energy [20–22]. This coupling between gas and power systems lays the groundwork for an integrated and resilient energy infrastructure capable of balancing intermittent renewables and achieving long-term sustainability goals.

This study focuses on evaluating the injection of hydrogen into natural gas supplies for regional power generation systems, simulating the operational performance and feasibility of hydrogen blending under various scenarios, quantifying the influencing factors, and conducting sensitivity analyses to assess system behavior under different blending strategies. Results inform gas-power sector integration design and provide technical insight for transitions towards low-carbon, hydrogen-enriched energy systems.

2. Literature review

Hydrogen blending into natural gas pipelines has attracted growing attention for decades. Most existing studies have focused on modeling and simulating the impact of hydrogen injection on the properties of the gas mixture within pipeline networks.

Tabkhi et al. [23] propose a steady-state optimization model utilizing a simplified gun-barrel network topology to investigate the impacts of hydrogen injection on single pipeline energy transmission rates and compression operation. Abeysekera et al. [24] adapt the graph-based model to analyze the effects of hydrogen injection from centralized and decentralized gas sources in the distribution networks. Adolfo and Carcasci [25] also investigate the location impact of hydrogen injection within low-pressure gas networks. They find that the node positions for hydrogen injection can affect the characteristics significantly within the network. Cheli et al. [26] develop a steady-state model of a natural gas distribution network on a smaller scale in Tuscany, Italy, to investigate how the injection of hydrogen produced from local renewable sources would influence gas properties when taking into account both the gas demand and electricity demand profiles. The study highlighted the need for an appropriate choice of the hydrogen injection nodes and a flexible control strategy. Despite the substantial progress in natural gas pipeline modeling, most conventional approaches rely on nodal balance equations built upon incidence matrix formulations. These methods, often coupled with nonlinear solvers such as Newton–Raphson, are effective for detailed simulations and operational control in small- to medium-scale networks [27]. However, when applied to large-scale regional systems, such as state-wide or national networks, these models face several critical limitations.

Timmerberg and Kaltschmitt [28] investigate the costs for producing hydrogen in North Africa and using existing pipelines operating between Algeria and Spain, Algeria and Italy, and Libya and Italy to transport hydrogen to central Europe with hydrogen blends of up to 10% by volume. Pellegrini et al. [29] perform an analysis with the intent of quantifying the amount of green hydrogen that could be produced and injected into the Italian natural gas grid without compromising its integrity or causing problems for end-users. As the concept of hydrogen blending moves from theoretical exploration toward practical implementation, numerous projects are now underway across the globe [30]. Regional-scale case studies have also emerged as a growing area of interest in recent years, aiming to evaluate the feasibility and performance of hydrogen integration under localized infrastructure, demand, and regulatory conditions. These kind of regional case projects and studies includes France [31,32], Italy [4,33,34], the United Kingdom [35], Germany [36], the United States [37–39], among others. However, these studies mainly discuss the potential of the economic aspect without considering the transformation and influence of end-users.

Many of these regional studies adopt coarse-grained approaches, relying on simplified assumptions for pipeline topology and energy flow paths. Transmission routes are often manually defined rather than derived from infrastructure-level data or optimization principles, limiting their ability to reflect the operational complexity of real-world networks. In addition, these studies tend to focus on single blending scenarios using empirical or phenomenological models and qualitative arguments to examine the physical and regulatory impacts of blending hydrogen and natural gas [40], lacking systematic comparisons across alternative strategies or sensitivity analyses that could reveal critical trade-offs and operational thresholds. As a result, a gap remains between current modeling efforts and the nuanced decision-making required for the practical deployment of hydrogen at scale.

Although interest in low-carbon hydrogen blending is accelerating, earlier research has typically focused on individual pipelines or assumed a uniform blend across an entire grid. As a result, there is still a significant lack of studies that explicitly identify the challenges and opportunities that may exist for hydrogen integration in a variety of regional NG transportation topologies, subject to gas quality constraints. Hence, in this work, well-established simulation techniques are utilized to explore indicative case studies for specific regions of California and draw broader conclusions about topological characteristics that could influence the hydrogen injection performance for the power generation sector. The contributions of this study include:

(1) California's natural gas transportation network in the power sector is reconstructed with the regional supply and decomposed into rooted tree structures that connect processing plants to power plants, allowing a topological analysis of the impacts of hydrogen mixing.

(2) Three coverage metrics — pathway, plant, and flow coverage — are defined and measured, and their explanatory capability is demonstrated in linking network topology to hydrogen penetration outcomes and heating-value variance across regions.

(3) Distributed, centralized, and optimization-based hydrogen injection strategies are systematically compared through a multi-objective optimization and simulation model, with trade-offs in penetration, coverage, and variance quantified across the Bay Area, Los Angeles, and Bakersfield.

(4) Siting heuristics based on lowest common ancestors and cross-tree nodes are introduced to balance hydrogen penetration, uniformity of the heating-value, and cost of the infrastructure.

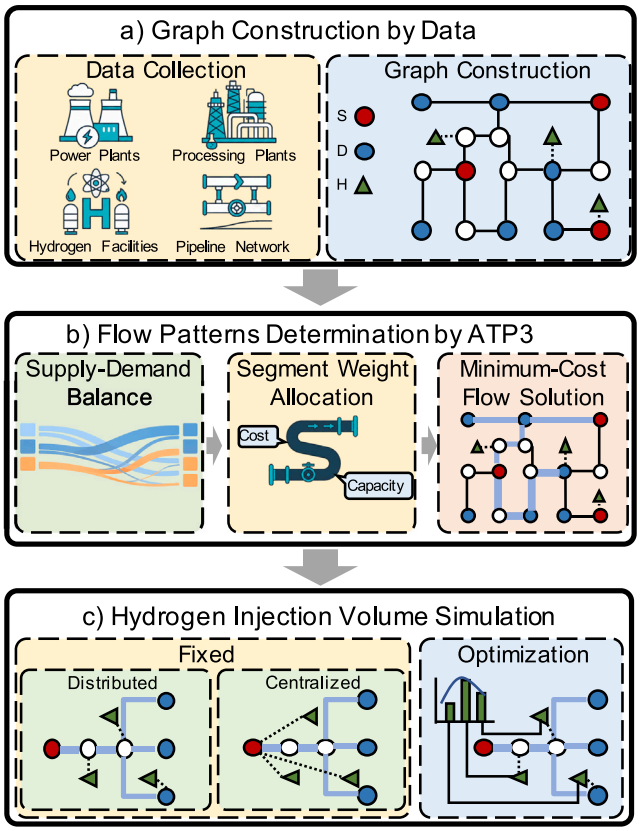

Fig. 1. Overall workflow of the modeling and analysis framework.

3. Methodology

To systematically evaluate the impacts of government subsidy schemes and hydrogen injection strategies on hydrogen penetration and end-user gas quality, this study performs region-scale simulations for three representative areas in California — the Bay Area, Los Angeles, and Bakersfield — chosen to capture distinct pipeline topologies and heterogeneous supply–demand characteristics. An overview of the methodological workflow is shown in Fig. 1. Briefly, the analysis proceeds in three stages. First, region-specific natural gas infrastructures are constructed from data and abstracted as graph-based pipeline networks, with facilities represented as nodes and pipelines as edges. Second, transportation pathways and flow patterns are identified across each network, enabling the estimation of flow rates both at nodes and along edges. Third, hydrogen injection locations and volumes are specified under different predefined hydrogen injection schemes. Subsequently, the resulting flow distributions are combined with hydrogen blending to quantify the heating-value delivered to end users and to evaluate regional hydrogen penetration levels.

3.1. Graph construction by data

3.1.1. Data collection

Publicly available data on power plants, gas processing plants, and hydrogen facilities (including their coordinates and capacities) are adopted to trace gas flows and then simulate hydrogen injection effects. Power generation data and gas processing data were sourced and extracted primarily from the Homeland Infrastructure Foundation Level Database and the US Energy Information Administration [41–43] in 2022, respectively. The hydrogen facility data and pipeline network data were sourced primarily from the National Renewable Energy Laboratory [44]. According to the data adopted, there are 285 power plants with a consumption capacity of 2125.95 MMscf/d and 18 processing plants with a processing capacity of 599.95 MMscf/d in California. There are 35 hydrogen facilities distributed in California.

3.1.2. Graph construction

According to the pipeline data, letting the network be represented by a weighted graph $G = (N, E, W)$, where N is the set of nodes and E is the set of pipeline edges. W represents the weight w_{ij} of each edge $e_{ij} \in E$ connects two nodes (n_i and n_j). The assets, including processing plants S, power plants D, and hydrogen facilities H, are mapped onto the nodes N of G so that they become part of the node set ($S \subseteq N$, $D \subseteq N$, $H \subseteq N$). Each asset is associated with a specific node in the graph. If an asset is physically located at an existing pipeline node, it is directly mapped to that node. Otherwise, the asset is linked to the nearest pipeline node by adding a connector edge representing a short feeder pipeline. As a result, any route from a processing plant to a power plant will correspond to a path through the graph, and any hydrogen facility is connected into the graph for injection.

3.2. Transportation pathways and patterns determination

After the graph is constructed, transportation pathways and patterns are identified using a graph-based optimization approach proposed by the authors, which is named Algorithm for Transportation Pathways and Patterns through Pipeline network (ATP3) [45]. The procedure consists of three sequential stages: supply–demand balance, segment weight allocation, and minimum-cost flow (MCF) problem solution. The steady-state assumption is adopted because processing and consumption data are statistical snapshots and do not support transient analysis. As the primary objective of this study is to evaluate how hydrogen injection affects heating-value and system-level penetration under different scenarios — excluding transit-related factors such as pressure — a steady-state framework is considered appropriate and sufficient for the intended analysis.

3.2.1. Supply–demand balance

In practice, reported supply and demand data are often imbalanced due to incomplete coverage, aggregation effects, or data uncertainty. To ensure a consistent point-level allocation, supply–demand balance is enforced using an entropy-weight-based allocation strategy. Briefly, multiple operational indicators are evaluated for each supply node and normalized to account for differences in magnitude and directionality. The information entropy of each indicator is then used to derive objective, data-driven weights, yielding a composite score that reflects the relative contribution potential of each supply node. These scores are subsequently scaled to allocate aggregate supply toward regional demand while respecting individual supply capacity constraints. The resulting allocation ratios are used as weighting factors for outgoing flows at supply nodes, thereby providing a balanced and capacity-consistent input for subsequent analysis.

3.2.2. Segment weight allocation

After reconciling supply and demand at the system level, each pipeline e_{ij} is characterized by both a transportation cost and a transportation capacity. Transportation cost is introduced to capture distance-dependent attributes such as transportation expenditure, energy consumption, or emissions intensity associated with gas transmission. Consistent with prior studies [46–48], these attributes are assumed to scale approximately linearly with both transported volume and transmission distance. Accordingly, the cost weight w_{ij} of a pipeline segment e_{ij} is represented by its physical length d_{ij}, which is computed using the Haversine formulation [49]:

$$\begin{cases} a = \sin^2\left(\frac{\Delta \text{lat}}{2}\right) + \cos(\text{lat}_i)\cos(\text{lat}_j)\sin^2\left(\frac{\Delta \text{lon}}{2}\right), \\ c = 2 \cdot \text{atan2}\left(\sqrt{a}, \sqrt{1-a}\right), \\ d_{ij} = R_{\text{Earth}} \cdot c, \end{cases} \tag{1}$$

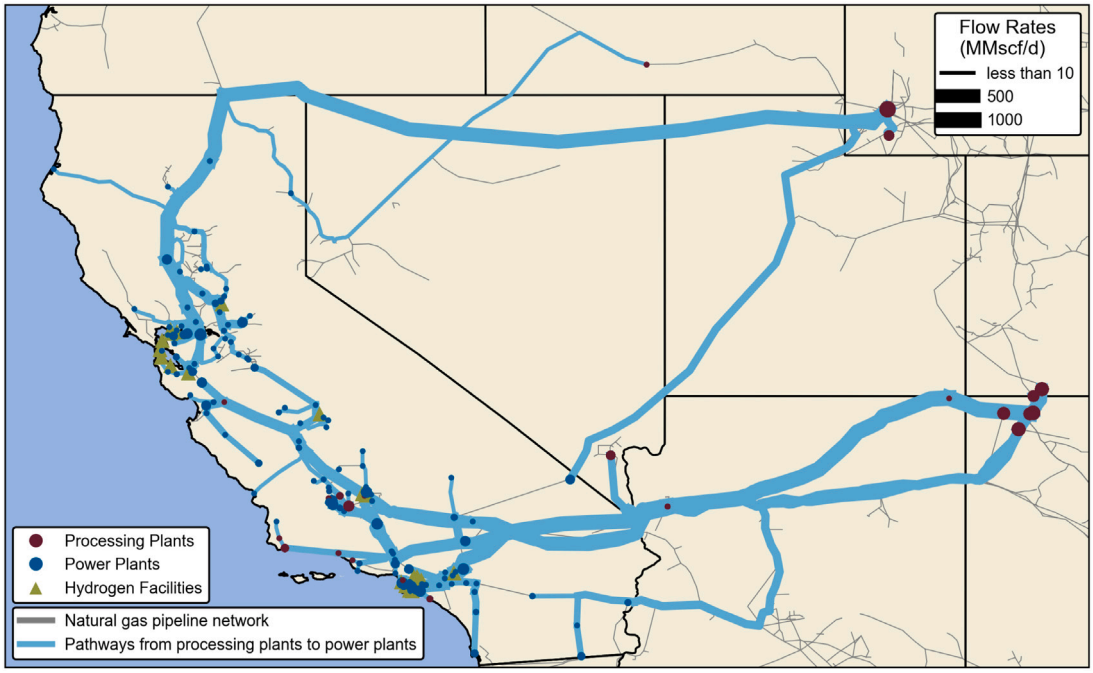

Fig. 2. Natural gas supply pathways to California power plants. The map illustrates the natural gas supply chain for California power generation sector: light blue lines represent simulated supply pathways from processing plants to power plants. Line thickness corresponds to the volumetric flow rate (MMscf/d), and node size reflects the facility's capacity. Green triangles denote the hydrogen facilities which are distributed in Bay Area, Los Angeles, and Bakersfield. (For interpretation of the references to color in this figure legend, the reader is referred to the web version of this article.)

where Δlat and Δlon denote the differences in latitude and longitude between nodes i and j, respectively, and R_{Earth} is the Earth's radius (set to 3960 miles in this study).

In addition to cost, each pipeline segment e_{ij} is associated with a capacity c_{ij}, representing the maximum volumetric throughput permitted by physical and operational constraints. Under this weight representation, the pipeline system is transformed into a weighted and capacity-constrained graph, providing the structural basis for subsequent shortest path identification and minimum-cost flow optimization.

3.2.3. Minimum-cost flow solution

Given the weighted and capacity-constrained graph, the determination of transportation pathways and flow patterns is formulated as an MCF problem. In the present study, regional gas throughput is substantially lower than nominal pipeline capacity, allowing capacity constraints to be treated as non-binding without loss of generality [50]. Under this assumption, natural gas is routed along minimum-cost paths between supply and demand nodes, consistent with the objective of minimizing distance-dependent transportation metrics. This enables the MCF problem to be decomposed into two tractable subproblems: (i) identification of shortest paths between all supply–demand pairs based on segment costs, and (ii) solution of a transportation problem over the reduced cost matrix. The transportation problem is formulated as:

$$\min: J = \sum_{i,j} w_{ij} x_{ij} \tag{2}$$

$$s.t. \begin{cases} \sum_j x_{ij} \le S_i & \forall i \\ \sum_i x_{ij} = D_j & \forall j \end{cases} \tag{3}$$

where w_{ij} represents the cost of transporting gas from source i to sink j, and x_{ij} is the capacity of gas transported, S_i represents the supply of node i; D_i denotes the demand of node j.

Since this is a linear optimization problem, the complete set of pipelines used for gas transport, along with the corresponding flow rates within each segment, can be obtained by linear programming. The natural gas supply pathways and patterns to California power plants, as obtained from ATP3, are shown in Fig. 2. There are 154 supply routes from processing plants to power plants, and the natural gas flow along each path and on each node can also be solved by aggregation.

3.3. Hydrogen injection simulation

3.3.1. Hydrogen injection mode

It can be seen in Fig. 2 that the positions of existing hydrogen facilities are distributed mainly in three regions (the Bay Area, Los Angeles, and Bakersfield), which have been selected as the case studies. The power plants in each region mainly receive natural gas from out-of-state or geographically distant processing plants. To facilitate subsequent simulations, spatial boundaries for the three regions are first defined. Then, processing plants located outside these boundaries are uniformly relocated to the nearest pipeline node at the intersection of their original transportation pathway and the regional boundary. The capacity assigned to each relocated point corresponds to the total natural gas flow through that node. To simplify representation, every processing plant within a specific region is denoted as a virtual processing node with vp.

Two hydrogen injection modes are considered in this study: a distributed and a centralized mode [24,51]. In the distributed injection scheme, hydrogen is injected at the node corresponding to each existing hydrogen facility as mapped onto the graph. In contrast, under the centralized mode, hydrogen is injected at the virtual processing node (vp) that is geographically closest (in network distance) to the specific hydrogen facility. Perfect mixing is assumed at each injection node.

The hydrogen concentration and the heating-value at the end of each transportation pathway (power plant inlet) can be calculated by Eqs. (4) and (5), respectively. These equations account for the cumulative effects of multiple hydrogen injection points along the pathway.

$$C_{H_2}^{\text{path}} = \frac{\sum_j Q_{H_2}^j}{Q^{\text{path}}} = \frac{\sum_j Q_{H_2}^j}{\sum_j Q_{H_2}^j + Q_{NG}^{\text{path}}} \tag{4}$$

$$HV^{\text{path}} = C_{H_2}^{\text{path}} \cdot HV_{H_2} + (1 - C_{H_2}^{\text{path}}) \cdot HV_{NG} \tag{5}$$

where $Q^{j}_{H_2}$ represents hydrogen injection volume at injection node j along the pathway, Q^{path}_{NG} represents natural gas volume along the pathway, Q^{path} represents gas mixture volume at the power plant inlet, $C^{\text{path}}_{H_2}$ represents hydrogen concentration reaching the power plant via this pathway, HV^{path} represents heating-value of the gas mixture at the power plant inlet.

The hydrogen concentration and heating-value of the gas received by each power plant are then computed by aggregating the gas inflows from each incoming pathway i, using a weighted average based on the flow contributions of each pathway:

$$C^{\text{plant}}_{H_2} = \frac{\sum_i Q^i \cdot C^i_{H_2}}{\sum_i Q^i} \tag{6}$$

$$HV^{\text{plant}} = C^{\text{plant}}_{H_2} \cdot HV_{H_2} + (1 - C^{\text{plant}}_{H_2}) \cdot HV_{NG} \tag{7}$$

where Q^i denotes gas flow rate along pathway i, $C^i_{H_2}$ denotes hydrogen concentration reaching the power plant via pathway i, $C^{\text{plant}}_{H_2}$ denotes effective hydrogen concentration received by the power plant, HV^{plant} denotes effective heating-value received by the power plant.

3.3.2. Simulation case design: distributed injection

Scenario I is the distributed hydrogen injection scheme. The injection volume at each location is set to 5% of the natural gas volumetric flow rate through this node before any injection. The injections are assumed to be operated simultaneously. To assess the system-level impact of hydrogen injection, two key performance indicators are considered in this paper:

1. Variance of heating-values at power plant inlets (V). This metric quantifies the uniformity of gas quality received by end users. A lower variance indicates a more uniform energy content across the region's power plants, which is desirable for combustion stability and operational predictability [52,53]. The variance is calculated as follows:

$$V = \text{Var}(HV^{\text{plant}}) = \frac{1}{N}\sum_{k=1}^{N}\left(HV^{\text{plant}}_k - \bar{HV}^{\text{plant}}\right)^2 \tag{8}$$

where HV^{plant}_k is the heating-value of the gas in power plant k, $\bar{HV}^{\text{plant}}$ is the average heating-value across all N power plants, N is the number of power plants in the region.

2. Regional hydrogen penetration rate (P). This metric reflects the overall proportion of hydrogen in the gas mixture consumed across the region. It serves as a proxy for the decarbonization potential of hydrogen blending. The penetration rate is computed as a flow-weighted average of hydrogen concentration across all power plants:

$$P = C^{\text{region}}_{H_2} = \frac{\sum_{k=1}^{N} Q_k \cdot C^{\text{plant}}_k}{\sum_{k=1}^{N} Q_k} \tag{9}$$

where C^{plant}_k represents the hydrogen concentration in power plant k, Q_k represents the total gas flow into power plant k, N represents the number of power plants in the region.

While higher regional penetration rates are desirable from a decarbonization standpoint, they are subject to practical constraints such as safety regulations, pipeline material compatibility, and policy limits on maximum allowable hydrogen blending ratios [30].

3.3.3. Simulation case design: centralized injection

Scenario II is the centralized hydrogen injection scheme building on the results from Scenario I. To ensure a fair comparison between the two schemes, the same amount of hydrogen injection volume is maintained, thus preserving the overall regional penetration rate. Instead of injecting hydrogen at the previous nodes, each facility's allocated injection volume is rerouted to the source up node on the pathway that serves as a centralized injection hub. The injected hydrogen is then distributed downstream from the up nodes to the connected power plants via the obtained gas flow pathways.

3.3.4. Simulation case design: injection volume optimization

Scenario III is extended from Scenario I by applying an optimization framework to determine the hydrogen injection volumes at each distributed node. Unlike the fixed 5% injection rate used previously, this approach allows injection volumes to vary across nodes, enabling a multi-objective optimization to balance gas quality uniformity and decarbonization potential. The control variables $\mathbf{q}$ are a set of injection amounts of each hydrogen facility seen in Eq. (10). The optimization target is to simultaneously minimize the variance of heating-values received by power plants (V) and maximizes the regional hydrogen penetration rate (P). These two objectives can be combined into a single scalarized cost function using a tunable weighting parameter $\alpha \in [0, 1]$ [54,55], the objective function is defined as in Eq. (11).

$$\mathbf{q} = \begin{bmatrix} Q^1_{H_2} & Q^2_{H_2} & \cdots & Q^J_{H_2} \end{bmatrix} \in \mathbb{R}^{1\times J} \tag{10}$$

$$\begin{aligned} \min_{\mathbf{q}\in\mathbb{R}^J} \quad & \alpha \cdot V(\mathbf{q}) - (1-\alpha)\cdot P(\mathbf{q}) \\ \text{s.t.} \quad & 0.01 \cdot Q^j_{NG} \le Q^j_{H_2} \le 0.2 \cdot Q^j_{NG} \quad \forall j = 1, \ldots, J \\ & C^{\text{plant},k}_{H_2}(\mathbf{q}) \le 0.25 \quad \forall k = 1, \ldots, N \end{aligned} \tag{11}$$

where: $Q^j_{H_2}$ denotes the hydrogen injection volume at node j, Q^j_{NG} denotes the natural gas flow at injection node j, $V(\mathbf{q})$ denotes the variance of heating-values across all power plants, $P(\mathbf{q})$ denotes the regional hydrogen penetration rate, $C^{\text{plant},k}_{H_2}(\mathbf{q})$ is the hydrogen concentration in power plant k, N is the total number of power plants in the study region, J is the total number of hydrogen injection nodes

The first constraint limits the hydrogen injection volume at each node to 1%–20% of the local natural gas volume, primarily reflecting technical and safety considerations such as compressor tolerance and blending stability [18,19,56,57]. The second constraint imposes an upper bound of 25% on the hydrogen concentration at the inlet of each power plant, representing a safety-related limit derived from turbine and combustion compatibility [58]. In this study, these bounds are uniformly applied across all nodes and facilities as a modeling simplification, although the proposed framework can accommodate node-specific limits once detailed operational data become available.

To solve the optimization problem defined in Eq. (11), the Sequential Least Squares Programming (SLSQP) algorithm implemented in `scipy.optimize.minimize` is employed. SLSQP is a gradient-based constrained optimization method that is well-suited for problems with nonlinear objectives and inequality constraints. In our case, both the heating-value variance and the hydrogen penetration rate are smooth. Differentiable functions and the constraint structure are convex. These properties make SLSQP an appropriate and efficient choice for solving this problem.

A Pareto front of each region is first generated by solving the optimization problem under varying values of α. This allows us to capture the full spectrum of feasible solutions that balance the competing objectives of minimizing V and maximizing P. To further explore the practical implications, three representative policy scenarios that reflect different levels of government subsidies for hydrogen injection are simulated:

- **High subsidy:** This scenario reflects strong policy support for hydrogen blending, such as direct subsidies or carbon credits. A higher emphasis is placed on maximizing hydrogen penetration with a lower value of α.
- **Medium subsidy:** This scenario represents a balanced policy environment in which both gas quality uniformity and decarbonization are equally valued.
- **Low subsidy:** This scenario reflects limited policy support or technical caution. The priority is placed on maintaining uniform gas quality with a higher value of α.

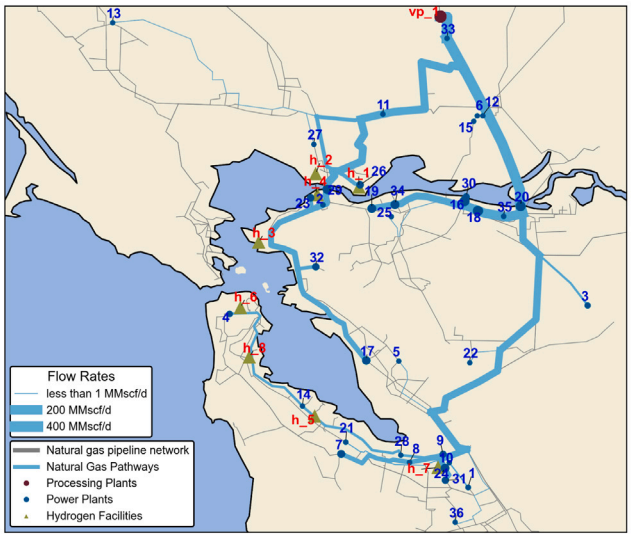

Fig. 3. Natural gas transmission pattern and hydrogen facilities in the Bay Area region. The pattern contains one *vp* (red dot), 36 power plants (blue dots), and 8 hydrogen facilities (green triangles). A total of 36 gas transmission pathways (blue lines) are established, with line widths proportional to flow rates. All power plants are connected to the network via a tree-like structure rooted at the single *vp* node. (For interpretation of the references to color in this figure legend, the reader is referred to the web version of this article.)

4. Results and discussion

Since the primary objective is to investigate how hydrogen injection performance is shaped by both policy incentives and the underlying gas transportation network topology, the results of Scenario I, II, and III for each of the three regions will be first illustrated. Then a cross-regional discussion will be conducted to compare different network structures and deliver policy recommendations.

4.1. Northern California (Bay Area)

The natural gas transmission patterns and infrastructure layout for the Bay Area region are shown in Fig. 3. Notably, all power plants in this region are supplied from a single source *vp*1, forming a classic tree-like topology.

4.1.1. Comparison of distributed and centralized injection

Fig. 4 compares the heating-values received by power plants in the Bay Area under distributed and centralized hydrogen injection scenarios. In the distributed case (left panel), spatial heterogeneity in injection results in a wide range of heating-values across the network, with a calculated variance of 0.596 MJ/m^3. The variation is largely driven by numbers of upstream hydrogen injection points. In contrast, under centralized injection (right panel), hydrogen is blended at a single *vp* node before distribution, resulting in a uniform heating-value across all downstream power plants. The variance in this case is effectively zero.

To quantitatively evaluate the extent of hydrogen distribution in the network, three coverage metrics are defined as:

(1) *pathway coverage ratio* (R_{path}), defined as the proportion of hydrogen-carrying pathways among all pathways;

(2) *plant coverage ratio* (R_{plant}), defined as the fraction of power plants that receive hydrogen-blended gas;

(3) *flow coverage ratio* (R_{flow}), defined as the percentage of total natural gas flow volume that passes through hydrogen-injected segments.

When each hydrogen facility injects hydrogen at a fixed rate of 5% of the local natural gas flow, the resulting regional hydrogen penetration reaches 1.11%. Fig. 5 illustrates the gas and hydrogen flow received at each power plant under both distributed and centralized injection scenarios. In the distributed injection scenario (left panel), R_{path} and R_{plant} are both 22.2% (8 out of 36), and R_{flow} is 18.6% (63.97 out of 343.77 MMscf/d). This limited spatial coverage results in non-uniform heating-values across the region. In contrast, under centralized injection (right panel), the single tree-like network topology enables the hydrogen injected at *vp* node to reach all power plants (coverage ratio to be 100%), resulting in a fully uniform gas mixture.

4.1.2. Injection flow optimization

Building on the distributed injection, the hydrogen injection volumes at each facility are optimized. The resulting Pareto front is shown in Fig. 6, highlighting the inherent trade-off between the two competing objectives: minimizing the variance of heating-values and maximizing the regional hydrogen penetration rate.

As the figure illustrates, improvements in hydrogen penetration come at the cost of reduced gas quality uniformity, and vice versa. To examine the practical implications of this trade-off under different policy environments, three representative subsidy regimes — *low*, *medium*, and *high* — corresponding to points along the Pareto frontier. These regimes reflect varying degrees of incentive for hydrogen adoption, and lead to different optimal injection patterns in the network, as discussed in subsequent analyses.

The resulting heating-value distributions under different subsidy regimes are shown in Fig. 7. As policy support increases from low to high subsidy levels, the optimized hydrogen injection volumes also increase accordingly. This results in a gradual rise in regional hydrogen penetration, but also leads to a corresponding increase in the variance of heating-values across power plants.

However, the magnitude of change in both objectives remains relatively modest. As illustrated by the gas flow and hydrogen ratio results in Fig. 8, the power plants that receive hydrogen injections have relatively low natural gas consumption. The natural gas flow coverage ratio is only 18.6%. Consequently, even under the high subsidy scenario, the overall regional hydrogen penetration remains below 4%.

The optimized hydrogen injection ratios at each facility are shown in Fig. 9. By integrating these results with the network flow patterns, following key observations are derived:

First, hydrogen facilities with higher natural gas throughput play a dominant role in determining the overall injection impact, regardless of the policy scenario. Their injection levels are more likely to approach the upper bound in high subsidy settings and contribute more substantially to regional hydrogen penetration.

Second, power plants that experience the largest changes in gas composition due to hydrogen injection can be broadly classified into two categories: (1) those located downstream of multiple hydrogen facilities — such as plant 4 (influenced by upstream facilities h_5, h_6, and h_8) and plant 26 (influenced by h_1 and h_2); and (2) those covered by major flow corridors linked to high-throughput facilities — such as plants 17 and 32 (both downstream of h_3), and plants 24 and 31 (downstream of h_7).

4.2. Southern California (Los Angeles)

The natural gas transmission patterns and infrastructure layout for the Los Angeles (LA) region are shown in Fig. 10. The transportation topology is more complicated than that of Bay Area with two outside sources (*vp*_4 and *vp*_5) and three local sources (*vp*_1, 2, and 3).

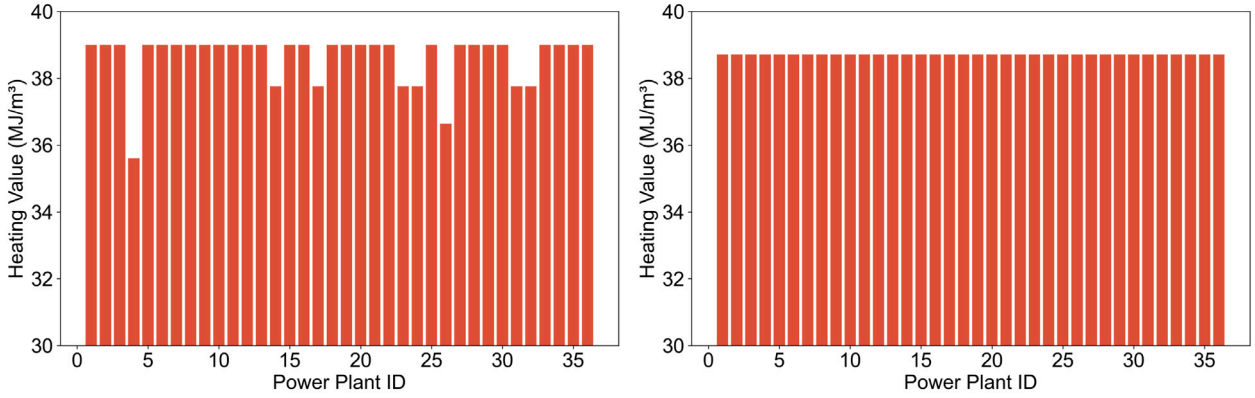

Fig. 4. Heating-value distribution at power plants in the Bay Area. Left: Distributed injection leads to substantial variability (variance = 0.596 MJ/m^3), reflecting spatial differences in injection intensity and network topology. The degree of heterogeneity is influenced by the number and placement of upstream hydrogen facilities. **Right:** Centralized injection results in a uniform heating-value (variance = 0), as hydrogen is blended at a single upstream node.

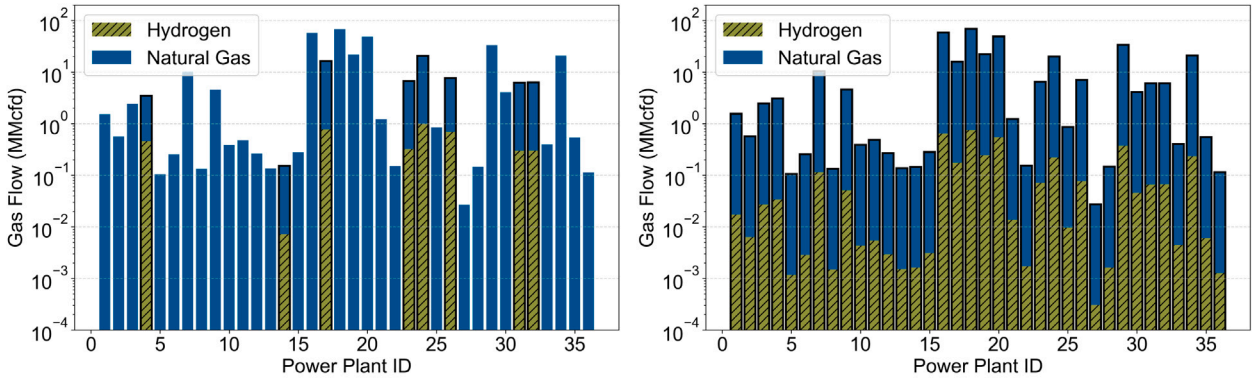

Fig. 5. Natural gas and hydrogen flow received by each power plant in the Bay Area. Bars outlined in black indicate power plants that are covered by hydrogen injection. **Left:** Distributed injection: only power plant 4, 14, 17, 23, 24, 26, 31, and 32 are covered by the upstream hydrogen injection. **Right**: Centralized injection: enables full network coverage (36/36 power plants) due to the single tree-like topology.

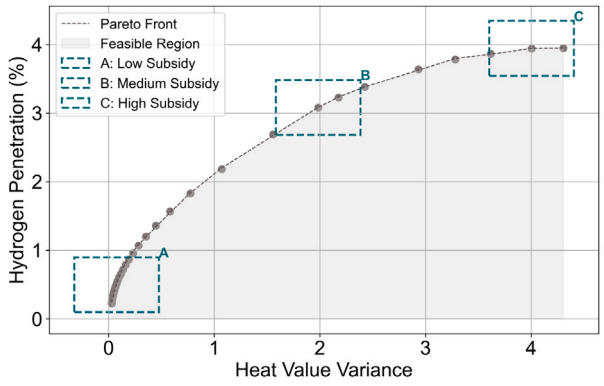

Fig. 6. Pareto front of heating-value variance versus hydrogen penetration in Bay Area. The shaded region indicates the feasible space. Three policy regimes are highlighted: **A** (low subsidy) prioritizes gas quality uniformity, **B** (medium subsidy) balances both objectives, and **C** (high subsidy) emphasizes hydrogen penetration. Each corresponds to a different weighting of the multi-objective optimization.

4.2.1. Comparison of distributed and centralized injection

Fig. 11 compares the heating-value distributions received by power plants in LA under distributed and centralized hydrogen injection scenarios. In this region, distributed case (left panel) also shows a larger variation than the concentrated case (right panel). This is primarily due to the rerouting of all hydrogen volumes to up_3 and up_4, from which the gas is uniformly redistributed across the network.

The transportation topology in this region can still be interpreted as a combination of several tree-like substructures, each rooted at a distinct up. When each power plant is supplied exclusively by a single root node, or by multiple root nodes with identical hydrogen concentrations, uniform heating-values can be maintained. However, if a power plant receives supply from multiple ups with different hydrogen concentrations, fluctuations in heating-value are likely to occur. Such deviations are evident in plant 16 (supplied by up_1 and 4), 31 (by up_2 and 4), and plant 38, 39, and 43 (by up_3 and 4), as well as plant 46 (by up_4 and 5).

When each hydrogen facility injects hydrogen at a fixed rate of 5% of the local natural gas flow, the resulting regional hydrogen penetration reaches 6.81%. Fig. 12 illustrates the gas and hydrogen flow received at each power plant under both distributed and centralized injection scenarios. In the distributed scenario (left panel), R_{path} is 76.9% (40 out of 52), R_{plant} is 81.25% (39 out of 48), and R_{flow} is 86.45% (413.51 out of 478.34 MMscf/d). In the centralized scenario (right panel), R_{path} is increased to be 82.69% (43 out of 52), R_{plant} is increased to be 87.5% (42 out of 48), and R_{flow} is increased to be 86.74% (414.90 out of 478.34 MMscf/d).

In the LA region, the gas transportation pattern is characterized by the presence of one tree-structured subnetwork that is largely isolated from the other tree structures. The overlap between this tree and the remaining network is limited primarily to peripheral or terminal

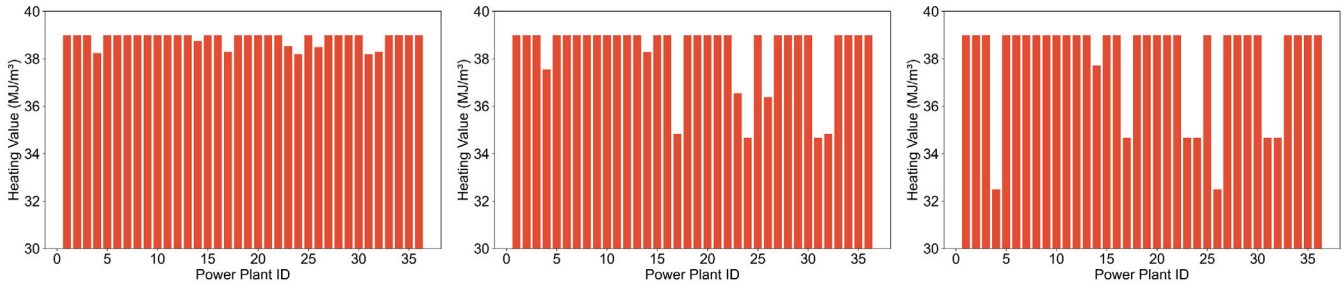

(a) Low Subsidy (b) Medium Subsidy (c) High Subsidy

Fig. 7. Natural gas and hydrogen flow received by each power plant in the Bay Area under different subsidies. (a). V: 0.075 MJ/m^3, P: 0.51%; (b). V: 1.984 MJ/m^3, P: 3.08%; (c). V: 4.00 MJ/m^3, P: 3.94%.

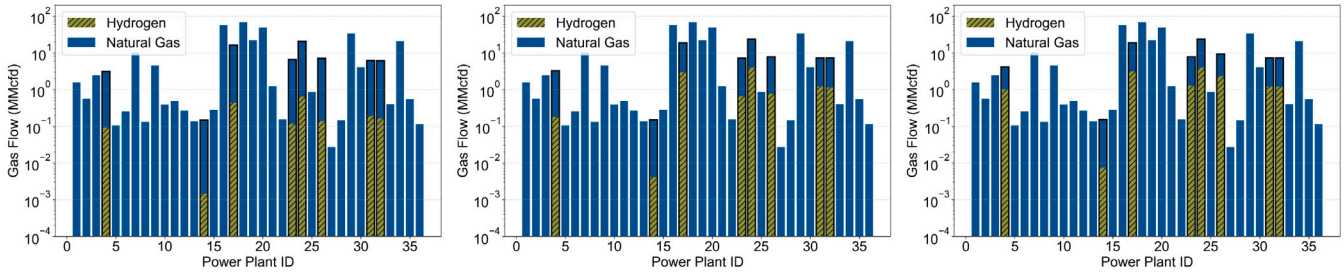

(a) Low Subsidy (b) Medium Subsidy (c) High Subsidy

Fig. 8. Heating-value distribution at power plants in the Bay Area under different subsidies. Bars outlined in black indicate power plants that are covered by hydrogen injection.

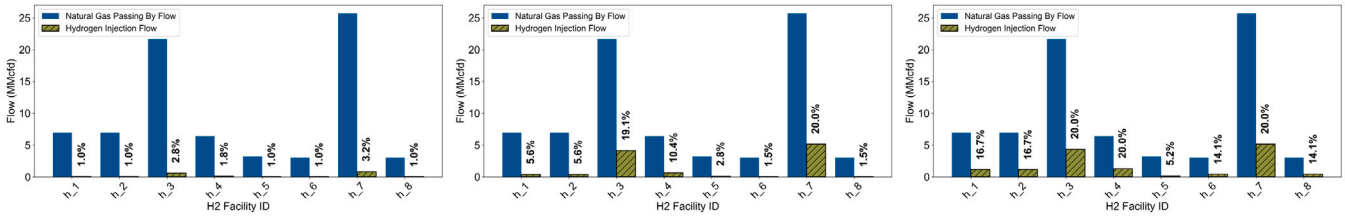

(a) Low Subsidy (b) Medium Subsidy (c) High Subsidy

Fig. 9. Hydrogen injection flow at each facility in the Bay Area under different subsidies. At the facility level, the blue bars indicate the natural gas flow passing through each hydrogen facility, while the yellow hatched bars represent the hydrogen injection volumes. The percentage values denote the optimized injection ratio at each facility, serving as the key control variable in the multi-objective optimization.

nodes, indicating minimal structural redundancy or intersection at higher hierarchical levels. This topological separation, combined with an uneven spatial distribution of hydrogen facilities — which do not cover the isolated subnetwork — limits the effectiveness of centralized injection in this region. As a result, despite implementing centralized blending, there is no significant improvement in hydrogen coverage, nor a corresponding enhancement in heating-value uniformity across the entire network.

4.2.2. Injection flow optimization

Building on the distributed injection, the hydrogen injection volumes at each facility are optimized. The resulting Pareto front is shown in Fig. 13, also highlighting the inherent trade-off between the two competing objectives.

The resulting heating-value distributions under different subsidy regimes are shown in Fig. 14. Increased policy support increases also results in a gradual rise in regional hydrogen penetration and a corresponding increase in the variance of heating-values. As the hydrogen blending volume increases, the resulting heating-values allows the power plants to be clearly grouped into several distinct clusters. This stratification arises from the fact that, hydrogen facilities in LA are predominantly located at higher-level nodes within the transportation tree. As a result, each injection point covers a larger number of downstream power plants, leading to similar heating-value trajectories and magnitudes within each group.

Under different policy scenarios, the variance of heating-values in LA ranges from 0 to 4.69 MJ/m^3, comparable to that observed in the Bay Area. However, the maximum hydrogen penetration in LA reaches 17.65%, which is significantly higher than that of the Bay Area. In addition to larger hydrogen coverage, this higher penetration can be attributed to the fact that several highest-consuming power plants (such as 12, 25, and 33) in LA are covered by hydrogen injection. As shown in Fig. 15, the inclusion of these major consumers under the hydrogen distribution path substantially amplifies the overall penetration rate, even under the existing blending constraints.

The optimized hydrogen injection ratios at each facility are shown in Fig. 16. It can also concluded that hydrogen facilities with higher natural gas throughput (h_7) play a dominant role in determining the overall injection impact.

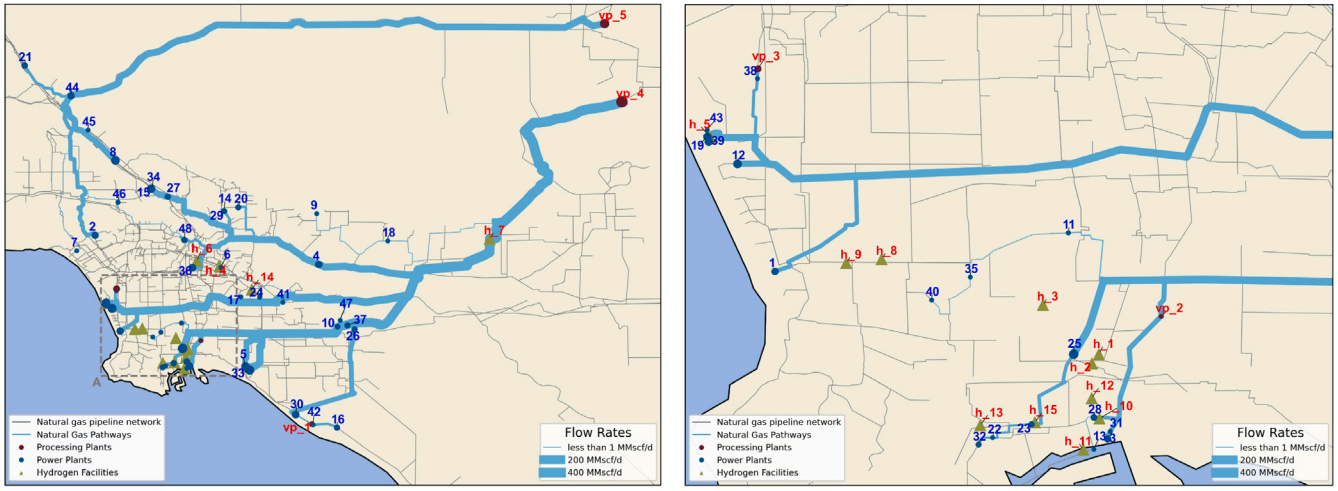

Fig. 10. Natural gas transmission pattern and hydrogen facilities in the LA region. Right is the zoomed in illustration of area **A** in **Left**. The pattern contains 5 *ups* (red dot), 48 power plants (blue dots), and 15 hydrogen facilities (green triangles). A total of 52 gas transmission pathways (blue lines) are established, with line widths proportional to flow rates. (For interpretation of the references to color in this figure legend, the reader is referred to the web version of this article.)

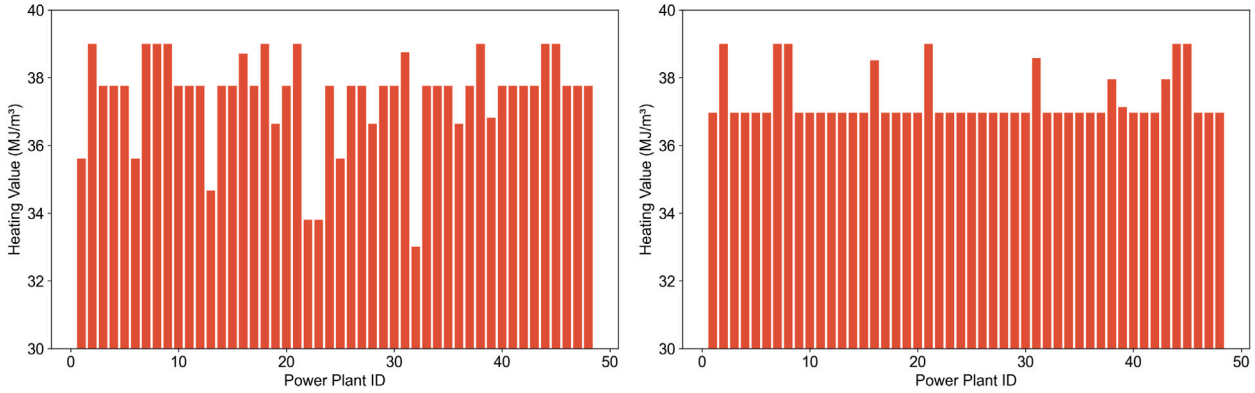

Fig. 11. Heating-value distribution at power plants in LA. Left: Distributed injection leads to substantial variability (variance = 1.961 MJ/m^3), reflecting spatial differences in injection intensity and network topology. The degree of heterogeneity is influenced by the number and placement of upstream hydrogen facilities. **Right:** Centralized injection results in a more uniform heating-value (variance = 0.529 MJ/m^3).

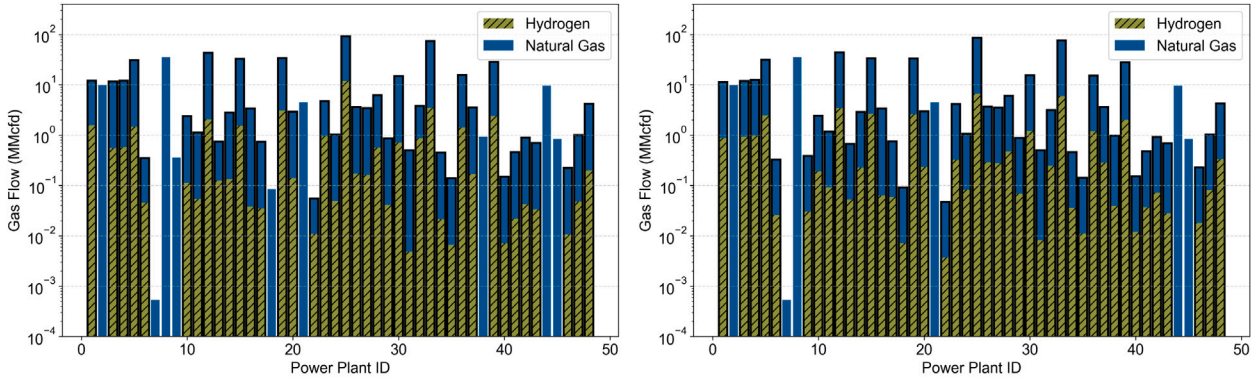

Fig. 12. Natural gas and hydrogen flow received by each power plant in LA. Bars outlined in black indicate power plants that are covered by hydrogen injection. **Left:** Distributed injection: power plant 2, 7, 8, 9, 18, 21, 38, 44, and 45 are not covered by the upstream hydrogen injection. **Right**: Centralized injection: power plant 2, 7, 8, 21, 44, and 45 are not covered by the upstream hydrogen injection. R_{plant} is improved from 81.25% to 87.5% by centralized injection, but there are still uncovered power plants because of the topology.

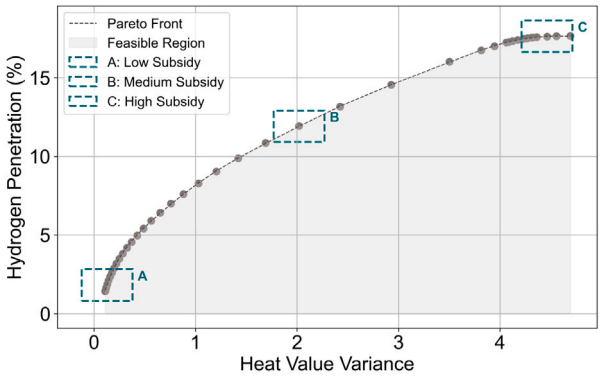

Fig. 13. Pareto front of heating-value variance versus hydrogen penetration in LA. The shaded region indicates the feasible space. Three policy regimes are highlighted: **A** (low subsidy) prioritizes gas quality uniformity, **B** (medium subsidy) balances both objectives, and **C** (high subsidy) emphasizes hydrogen penetration. Each corresponds to a different weighting of the multi-objective optimization.

4.3. Central California (Bakersfield)

The natural gas transmission patterns and infrastructure layout for the Bakersfield region are shown in Fig. 17. This region exhibits a distinct multi-source supply pattern, characterized by the presence of 9 vps. As a result, the overall transportation network is composed of nine tree-like structures, each rooted at a different vp node. This structure reflects a decentralized flow architecture, in which gas is distributed through multiple independent supply pathways rather than a single dominant source.

4.3.1. Comparison of distributed and centralized injection

Fig. 18 compares the heating-value distributions received by power plants in Bakersfield under distributed and centralized hydrogen injection scenarios. When each hydrogen facility injects hydrogen at a fixed rate of 5% of the local natural gas flow, the resulting regional hydrogen penetration only appears as 0.45%. Fig. 19 illustrates the gas and hydrogen flow received at each power plant under both distributed and centralized injection scenarios. In the distributed scenario (left panel), R_{path} is 8.0% (4 out of 50), R_{plant} is 7.14% (3 out of 42), and R_{flow} is 9.12% (45.25 out of 495.97 MMscf/d). In the centralized scenario (right panel), R_{path} is increased to be 56.0% (28 out of 50), R_{plant} is increased to be 61.9% (26 out of 42), and R_{flow} is increased to be 33.51% (166.18 out of 495.97 MMscf/d).

In the Bakersfield region, the limited number of hydrogen facilities — only three in total — plays a key role in shaping the injection performance. Facilities h_1 and h_3 are located near leaf nodes, close to individual power plants, while h_2 is also positioned at a relatively low-level node within the network hierarchy. As a result, under the distributed injection scenario, hydrogen coverage remains limited and spatially fragmented. However, centralized injection allows hydrogen to be rerouted to a higher-level node, significantly expanding its reach throughout the network. This shift substantially increases the overall hydrogen coverage and leads to a marked reduction in heating-value fluctuations across power plants.

4.3.2. Injection flow optimization

Building on the distributed injection, the hydrogen injection volumes at each facility are optimized. The resulting Pareto front is shown in Fig. 20, it can be seen that the two optimization objectives continue to exhibit a trade-off relationship. However, due to the limited spatial coverage of hydrogen in this region, adjusting the injection volumes alone yields only marginal improvements in either objective.

Table 1
Key topological characteristics comparison in three regions.

Category	Bay Area	Los Angeles	Bakersfield
Leaf nodes	36	48	42
Root nodes	1	5	9
Topology	Single-tree	Multi-tree, ~ isolated	Multi-tree, ~combined
Injection nodes	8	15	3
Facility position	Mid-level, low-level	High-level	Low-level
R_{path} (%)	22.2	76.9	8.0
R_{plant} (%)	22.2	81.25	7.14
R_{flow} (%)	18.6	86.45	9.12
Maximum P (%)	3.94	17.65	1.77

The current hydrogen infrastructure lacks sufficient reach to meaningfully influence gas quality or decarbonization potential. As such, further increases in regional penetration are unlikely to be achieved through injection control alone. Instead, expanding coverage through the strategic addition of new hydrogen facilities will be essential to improving performance in this region.

4.4. Cross-regional heterogeneity and topological interpretation

The results reveal substantial differences in hydrogen injection performance across the Bay Area, Los Angeles, and Bakersfield. Although the same modeling framework and injection strategies are applied in all cases, the observed variations in hydrogen penetration and heating-value uniformity indicate that regional outcomes are strongly conditioned by underlying topological heterogeneity. Table 1 summarizes the key topological characteristics of the three regions, providing a consolidated basis for cross-regional interpretation.

The Bay Area represents a highly centralized system characterized by a single-tree supply structure rooted at one virtual processing node. This configuration enables hydrogen injected at upstream locations to propagate uniformly to all downstream power plants once centralized injection is implemented, resulting in near-zero variance in heating-value. However, the limited coverage ratios constrain the achievable penetration level, even under optimized injection.

Los Angeles, by contrast, features a more complex multi-root topology with multiple high-capacity virtual processing nodes and substantial overlap between hydrogen facilities and major transmission corridors. This structural alignment allows hydrogen to access a large share of regional gas flow, leading to the highest penetration potential among the three regions. At the same time, partial isolation between subnetworks prevents complete homogenization of gas composition, such that residual heating-value variance persists even under centralized or optimized injection. This combination of high penetration and incomplete uniformity distinguishes Los Angeles from the other two regions.

The Bakersfield region exhibits a combined, multi-tree structure with sparse hydrogen infrastructure and injection points predominantly located at low-level or leaf nodes. Consequently, hydrogen coverage under distributed injection remains highly fragmented, and adjusting injection volumes alone yields limited system-wide impact. While centralized injection improves coverage by promoting hydrogen to higher-level nodes, overall penetration remains constrained by the limited number of facilities and their weak coupling to high-flow transmission paths. These characteristics make Bakersfield particularly sensitive to infrastructure siting rather than injection control.

Taken together, this cross-regional comparison demonstrates that differences in hydrogen injection performance arise primarily from topological heterogeneity—specifically, variations in network topology, coverage ratio metrics, and the relative positioning of hydrogen facilities. These observations motivate a more systematic examination of coverage as a unifying explanatory variable.

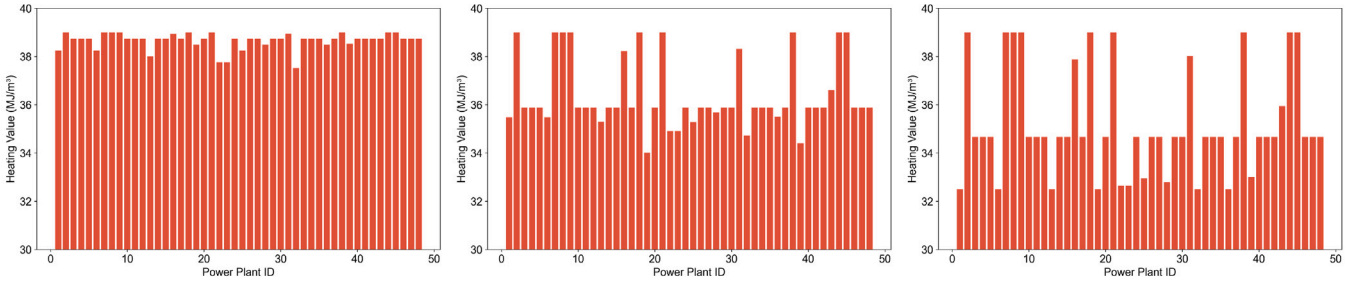

(a) Low Subsidy (b) Medium Subsidy (c) High Subsidy

Fig. 14. Natural gas and hydrogen flow received by each power plant in LA under different subsidies. (a). V: 0.11 MJ/m^3, P: 1.44%; (b). V: 2.02 MJ/m^3, P: 11.94%; (c). V: 4.69 MJ/m^3, P: 17.65%.

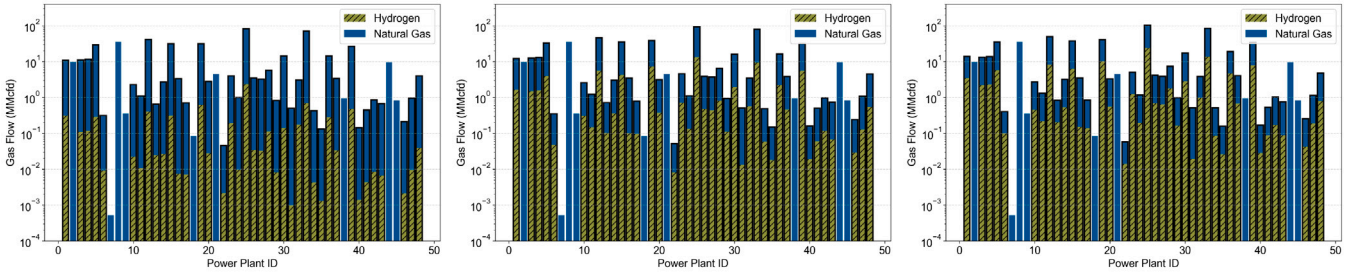

(a) Low Subsidy (b) Medium Subsidy (c) High Subsidy

Fig. 15. Heating-value distribution at power plants in LA under different subsidies. Bars outlined in black indicate power plants that are covered by hydrogen injection.

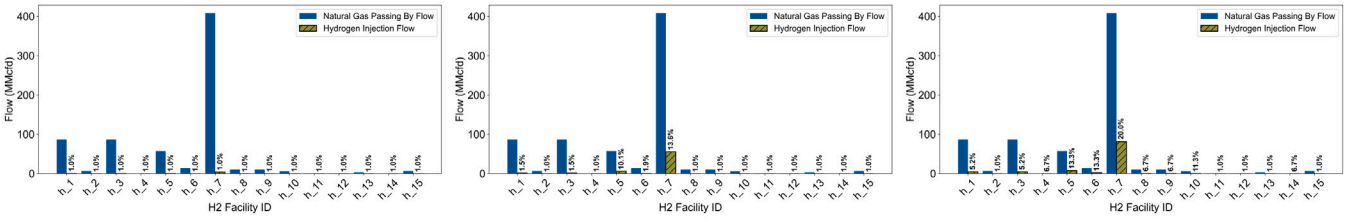

(a) Low Subsidy (b) Medium Subsidy (c) High Subsidy

Fig. 16. Hydrogen injection flow at each facility in LA under different subsidies. At the facility level, the blue bars indicate the natural gas flow passing through each hydrogen facility, while the yellow hatched bars represent the hydrogen injection volumes. The percentage values denote the optimized injection ratio at each facility, serving as the key control variable in the multi-objective optimization.

4.5. Sensitivity and interplay of coverage metrics

To clarify the distinct roles of the three coverage metrics (R_{path}, R_{plant}, and R_{flow}) introduced in this work, the behavior across the three representative regions using the existing simulation outcomes are examined. Although these scenarios were originally designed for qualitative comparison, together they span a sufficiently broad range of coverage values to reveal the governing relationships between the metrics and the resulting hydrogen blending performance.

4.5.1. Regional hydrogen penetration

Scenario III reveals the intrinsic penetration potential of each region when hydrogen supply amount are allowed to vary freely within existing topology and operational constraints. In this scenario, the three regions exhibit markedly different maximum achievable penetration levels: 3.94% in the Bay Area, 17.65% in Los Angeles, and 1.77% in Bakersfield. These differences closely follow their R_{flow}. Los Angeles, whose network structure allows hydrogen to access the vast majority of high-volume transport corridors, attains the highest penetration ceiling; the Bay Area, with moderate flow coverage, reaches an intermediate level; and Bakersfield, where only a small fraction of regional throughput is structurally reachable by hydrogen, shows the lowest ceiling. This relationship is illustrated in Fig. 21, which demonstrates the strong dependence of the achievable penetration envelope on flow coverage across the three regions.

This behavior highlights that R_{flow} governs not only the instantaneous penetration under a fixed injection volume, but also the upper boundary of penetration that the network can support when injection is optimized. Networks with higher flow coverage admit a substantially larger feasible region for hydrogen blending, enabling operators to raise penetration without breaching physical constraints. Conversely, networks with low flow coverage remain supply-constrained regardless of injection ratios. In this sense, R_{flow} acts as a structural enabler for both high-penetration blending and flexible optimal control.

4.5.2. Heating-value uniformity

In contrast, the uniformity of the delivered gas (quantified by the variance of heating-value V) is largely insensitive to R_{flow} but strongly conditioned by R_{plant} and R_{path}. Despite LA having far higher flow coverage (86.45%) than the Bay Area (18.6%), both regions exhibit

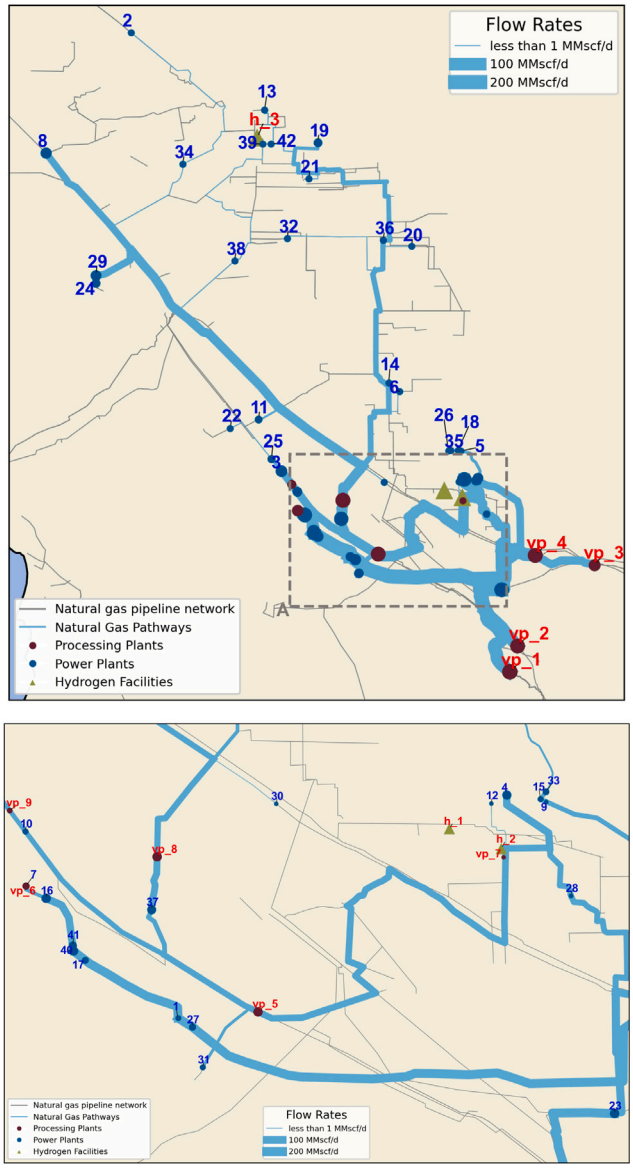

Fig. 17. Natural gas transmission pattern and hydrogen facilities in Bakersfield. Bottom is the zoomed in illustration of area **A** in **Top**. The pattern contains 9 *vp*s (red dot), 42 power plants (blue dots), and 3 hydrogen facilities (green triangles). A total of 50 gas transmission pathways (blue lines) are established, with line widths proportional to flow rates. (For interpretation of the references to color in this figure legend, the reader is referred to the web version of this article.)

similar range in heating-value variance V in Scenario III. This demonstrates that path and plant coverage dominate over flow coverage in controlling uniformity, particularly when injection is already able to access major flow corridors.

It can be seen in Fig. 22, transitioning from distributed to centralized injection leads to a marked increase in plant coverage across in Bay Area and Bakersfield (rising from 22.2% to 100%, and from 7.14% to 61.9%, respectively), while keeping the total injected hydrogen unchanged. This shift alone produces a substantial reduction in heating-value variance, underscoring the dominant role of end-user coverage in shaping network-wide uniformity. In the Bay Area, where the pipeline network exhibits a single-tree topology, raising R_{plant} to unity results in complete homogenization of the delivered gas, as all demand nodes become downstream of the same mixing point. Los Angeles and Bakersfield, where multiple source trees coexist and only partially overlap, also show large declines in variance when R_{plant} increases. However, some residual variance persists because end-users continue to draw from branches fed by distinct upstream sources. This behavior reflects a structural constraint: even with higher coverage, path segmentation limits the propagation of uniform hydrogen compositions across the entire network.

Together, these observations demonstrate that plant- and path-level coverage govern the spatial distribution of the blended gas rather than flow coverage. As R_{plant} and R_{plant} increase, hydrogen becomes accessible to a broader and more topologically coherent subset of end-users, allowing compositions to equilibrate more effectively across downstream consumers.

The three coverage metrics introduced in this study capture complementary aspects of how hydrogen disperses through a heterogeneous pipeline network. R_{flow} characterizes the share of regional throughput that is structurally reachable by hydrogen, thereby determining the maximum achievable penetration envelope under operational constraints. R_{plant} quantifies the fraction of end-users exposed to hydrogen-blended gas and is therefore the primary determinant of heating-value uniformity, while R_{path} captures topological coherence across flow corridors and governs the extent to which uniform compositions can propagate across sub-trees. These metrics offer a concise yet mechanistic representation of the structural factors that regulate hydrogen blending performance.

4.6. Discussion and recommendation

Based on the multi-scenario simulation results across diverse regional topologies, several practical insights emerge for designing hydrogen injection strategies and planning infrastructure investments. These findings offer actionable guidance for regulators, system operators, and infrastructure planners seeking to strike a balance between gas quality, decarbonization goals, and economic constraints.

(1) Maximize hydrogen coverage to reduce variance and enhance penetration. The results show that minimizing heating-value variance is primarily achieved by increasing the coverage of power plants and transmission pathways. When variance levels are comparable across scenarios, higher coverage leads to greater achievable regional hydrogen penetration. Ensuring that a larger portion of the network receives hydrogen-blended gas improves both uniformity and decarbonization potential.

(2) Leverage tree-structured flow patterns for strategic injection. All regional gas networks can be decomposed into collections of tree-structured subnetworks, each rooted at a processing plant (supply) and terminating at power plants (demand).

(3) Policy-relevant recommendation for hydrogen injection siting. Hydrogen injection siting should adopt a topology- and demand-aware strategy that balances system-wide effectiveness with economic feasibility. Upstream, high-level injection points offer less capital cost and improved control of gas-quality uniformity, but at the expense of higher transportation distances and operational risk. In contrast, downstream, low-level siting enables localized, lower-risk deployment with reduced delivery costs, yet provides limited system-wide influence and often requires a larger number of facilities to achieve comparable coverage, which increases the capital investment. New hydrogen facilities should be sited to balance the coverage efficiency, transportation cost, and capital investment. Three practical heuristics are recommended:

- Select the lowest-level common ancestor of uncovered power plants as candidate sites for injection points.
- Identify and target intersecting nodes across distinct tree structures as candidate sites to expand coverage with minimal new facilities.
- Place facilities upstream of high-demand power plants and along high-flow pathways to ensure greater coverage and maximize system-wide hydrogen penetration.

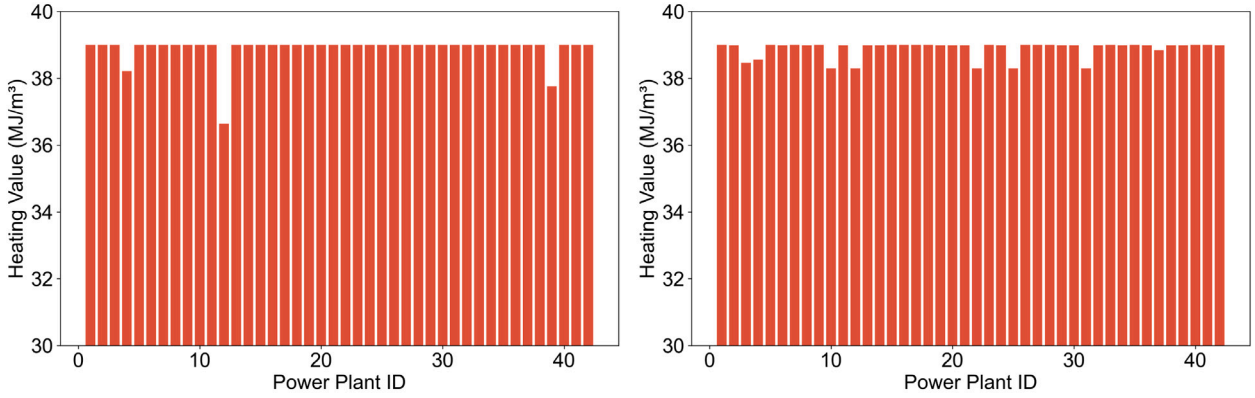

Fig. 18. Heating-value distribution at power plants in Bakersfield. Left: Distributed injection leads to a variance of 0.173 MJ/m^3. **Right:** Centralized injection leads to a variance of 0.057 MJ/m^3.

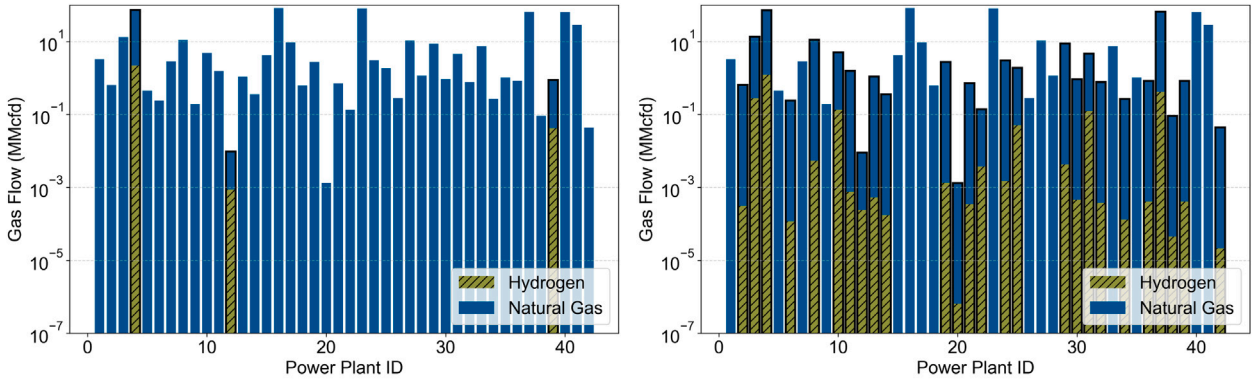

Fig. 19. Natural gas and hydrogen flow received by each power plant in Bakersfield. Bars outlined in black indicate power plants that are covered by hydrogen injection. **Left:** Distributed injection: h_1 only serves power plant 12, h_2 only serves power plant 4 and 12, h_3 only serves power plant 39. **Right**: Centralized injection: hydrogen is rerouted to *up* 5, 7 and 8 before distribution, significantly increased the coverage.

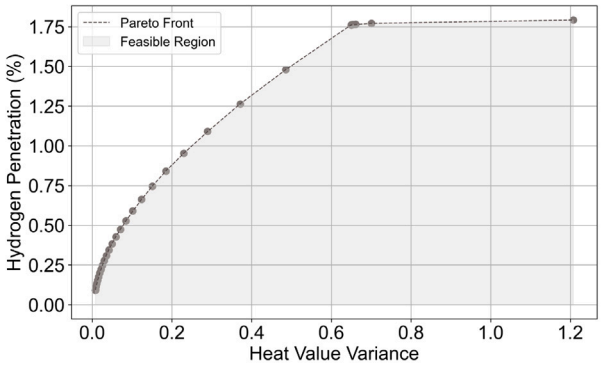

Fig. 20. Pareto front of heating-value variance versus hydrogen penetration in Bakersfield. The shaded region indicates the feasible space. Three policy regimes are highlighted: **A** (low subsidy) prioritizes gas quality uniformity, **B** (medium subsidy) balances both objectives, and **C** (high subsidy) emphasizes hydrogen penetration. Each corresponds to a different weighting of the multi-objective optimization.

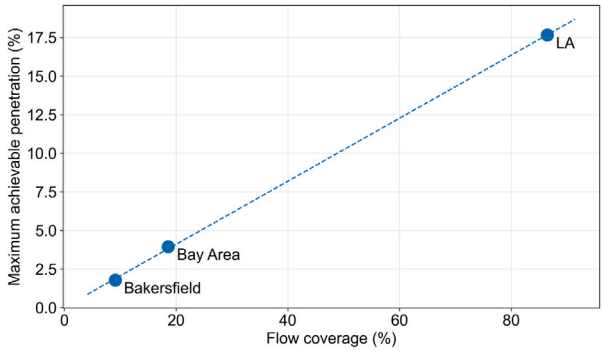

Fig. 21. Relationship between flow coverage R_{flow} and the achievable hydrogen penetration envelope under multi-objective optimization. Maximum penetration increases with the fraction of regional flow that is structurally reachable by hydrogen, reflecting topology-conditioned blending capacity.

5. Limitations and future work

5.1. Limitations

Steady-State Pipeline Assumption. This study assumes steady-state and equilibrium gas flows, which neglects transient fluctuations inherent in real natural gas networks. In practice, pipeline pressures, demands, and line-pack vary dynamically, influencing flow distribution and compressor loading [59]. While steady-state models are common for high-level planning and topology screening [60], they cannot capture short-term dynamics. This simplification was made to isolate long-term, topology-driven effects, as a preliminary study of detailed operational planning.

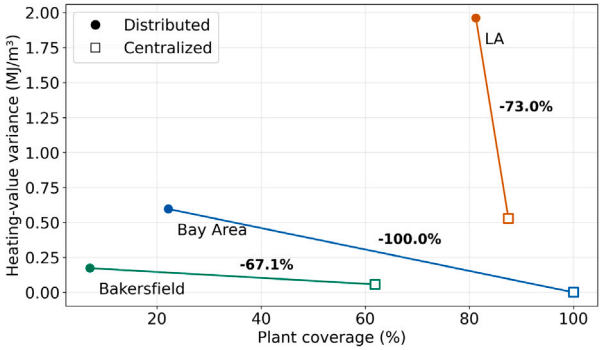

Fig. 22. Effect of increasing R_{plant} on heating-value uniformity. Lines indicate transitions from distributed to centralized injection. Increasing R_{plant} substantially reduces heating-value variance in all regions, with complete homogenization in the single-tree Bay Area network.

Simplified Hydrogen–Methane Mixing. The analysis assumes instantaneous and uniform hydrogen mixing within natural gas streams, disregarding incomplete mixing or stratification effects. In reality, buoyancy causes hydrogen to rise and methane to settle, forming concentration gradients under low-flow or laminar conditions [61]. Such stratification could create localized high-H_2 pockets, posing safety and materials risks. Computational Fluid Dynamics (CFD) simulations are not performed in this study to account for these effects. Instead, this paper focuses on macro-scale injection topology, assuming sufficient turbulence or engineered mixing devices to ensure homogeneity.

Absence of CFD-Based Risk Analysis. No high-resolution CFD or experimental risk assessments were performed to analyze localized phenomena such as flame flashback, leakage, or material degradation. These effects can influence the safety and reliability of hydrogen injection systems [61]. This study assumes that proposed configurations would later undergo site-specific CFD validation and compliance with engineering standards.

5.2. Future work

Building on these findings, future extensions will address the identified limitations through the following directions:

- Incorporate transient gas flow and time-series dynamics to assess operational stability under varying demand and supply conditions.
- Integrate CFD-derived correlations to capture hydrogen concentration gradients and ensure homogeneous blending.
- Embed cost functions for hydrogen production, transport, and infrastructure to balance technical optimality with financial feasibility.
- Couple topology optimization with material safety limits, CFD-based risk modeling, and contingency simulations to ensure safe operation under hydrogen blending.

By integrating these developments, the framework will evolve from a steady-state, topology-oriented tool into a comprehensive decision-support system that balances technical, economic, and safety objectives for hydrogen–natural gas co-transport.

6. Conclusion

This study presents a pathway-tracing-based framework for determining and optimizing natural gas transmission patterns and simulating hydrogen injection across California's power sector. By integrating spatial infrastructure data with flow optimization and injection modeling, this paper evaluate the gas quality and decarbonization performance under various blending strategies in three representative regions: the Bay Area, Los Angeles, and Bakersfield. Key insights are summarized as follows:

(1) Tree-based network decomposition. All regional transmission networks can be effectively decomposed into a collection of tree-like structures, each rooted at a processing plant (supply) and terminating at one or more power plants (demand). Hydrogen injected at any node within such a tree propagates downstream, influencing all descendant nodes—an essential property for targeting specific areas or clusters.

(2) Coverage as a control lever. The degree of regional hydrogen penetration and heating-value uniformity is tightly linked to what we define as *coverage*. This paper proposes three distinct metrics of coverage: (1) pathway coverage—the fraction of gas transmission paths intersected by hydrogen; (2) power plant coverage—the fraction of end users receiving hydrogen-blended gas; and (3) flow coverage—the percentage of total gas volume exposed to hydrogen. Enhancing any of these coverage dimensions enables broader and more balanced decarbonization.

(3) Policy-informed infrastructure recommendations. This paper introduces a set of siting, promotion, and optimization strategies to balance heating-value stability, hydrogen penetration, and deployment cost. These strategies account for regional topological sensitivity, spatial equity, and cost-risk trade-offs—offering actionable guidance for future hydrogen infrastructure planning under both technical and policy constraints.

Taken together, this framework offers a scalable approach to analyzing hydrogen injection impacts under realistic gas transmission constraints. It also provides a principled basis for siting and regulating hydrogen blending infrastructure that aligns with California clean energy transition goals.

CRediT authorship contribution statement

Zemin Eitan Liu: Writing – original draft, Visualization, Validation, Software, Methodology, Investigation, Formal analysis, Data curation, Conceptualization. **Zhenlin Chen:** Writing – review & editing, Visualization, Data curation. **Wennan Long:** Writing – review & editing, Project administration, Methodology. **Liang Jing:** Validation, Formal analysis, Data curation. **Diego Moya:** Visualization, Validation, Resources. **Bo Ren:** Resources, Data curation. **Farah Ramadan:** Validation, Project administration. **Abdulelah S. Alshehri:** Writing – review & editing, Project administration, Methodology. **Mohammad S. Masnadi:** Writing – review & editing, Validation, Supervision, Project administration, Funding acquisition, Conceptualization.

Declaration of competing interest

The authors declare that they have no known competing financial interests or personal relationships that could have appeared to influence the work reported in this paper.

Acknowledgments

The authors extend their appreciation to King Saud University for funding this research through the Ongoing Research Funding Program (ORF-2025-1445), King Saud University, Riyadh, Saudi Arabia. Dr. Zemin E. Liu also thanks Aramco America (Michigan office) for providing financial support.

References

[1] Ruth MF, Jadun P, Gilroy N, Connelly E, Boardman R, Simon A, Elgowainy A, Zuboy J. The Technical and Economic Potential of the H2 @Scale Hydrogen Concept Within the United States. Tech. rep., National Renewable Energy Lab.(NREL), Golden, CO (United States); 2020.

[2] Masnadi MS, Long W, Jing L, Liu ZE, Jabbar MY, Chen Z, Moya D, Ren B, Ma H, Littlefield J, Ramadan F, Al-Qahtani A, Guan D, Bi XT, Bergerson J, Ravikumar AP, Brandt A, El-Houjeiri H. Global carbon intensity of lng value chain amid intensifying energy security and climate trade-offs. 2025, http://dx.doi.org/10.21203/rs.3.rs-7255872/v1.

[3] Guo Z, Liu Z, Shuai S. Evolution and future development of vehicle fuel specification in China. In: SAE powertrains, fuels & lubricants digital summit. SAE Technical Paper 2021-01-1201, SAE International; 2021.

[4] Bellocchi S, De Falco M, Facchino M, Manno M. Hydrogen blending in Italian natural gas grid: scenario analysis and LCA. J Clean Prod 2023;416:137809.

[5] Mahajan D, Tan K, Venkatesh T, Kileti P, Clayton CR. Hydrogen blending in gas pipeline networks—a review. Energies 2022;15(10):3582.

[6] Van Wijk A, Chatzimarkakis J. Green hydrogen for a European green deal a 2x40 GW initiative. Hydrog Eur 2020;41–p.

[7] Albertus P, Manser JS, Litzelman S. Long-duration electricity storage applications, economics, and technologies. Joule 2020;4(1):21–32.

[8] GRTgaz IB, France-GRDF GRD, Terega EV, France S, Nordling RR, Reseau G, Non SPdEG, et al. Technical and economic conditions for injecting hydrogen into natural gas networks-Final report June 2019. Tech. rep., GRTgaz, Immeuble Bora, 6, rue Raoul-Nordling, 92277 Bois-Colombes Cedex (France); 2019.

[9] Maroufmashat A, Fowler M. Transition of future energy system infrastructure; through power-to-gas pathways. Energies 2017;10(8):1089.

[10] Chiang N-Y, Zavala VM. Large-scale optimal control of interconnected natural gas and electrical transmission systems. Appl Energy 2016;168:226–35.

[11] Correa-Posada CM, Sanchez-Martin P. Integrated power and natural gas model for energy adequacy in short-term operation. IEEE Trans Power Syst 2014;30(6):3347–55.

[12] Mariani A, Unich A, Minale M. Combustion of hydrogen enriched methane and biogases containing hydrogen in a controlled auto-ignition engine. Appl Sci 2018;8(12):2667.

[13] Lyu M, Zhang C, Bao X, Song J, Liu Z. Effects of the substitution rate of natural gas on the combustion and emission characteristics in a dual-fuel engine under full load. Adv Mech Eng 2017;9(12):1687814017747158.

[14] Jia G, Lei M, Li M, Xu W, Li R, Lu Y, Cai M. Hydrogen embrittlement in hydrogen-blended natural gas transportation systems: A review. Int J Hydrog Energy 2023;48(82):32137–57.

[15] Wu X, Zhang H, Yang M, Jia W, Qiu Y, Lan L. From the perspective of new technology of blending hydrogen into natural gas pipelines transmission: Mechanism, experimental study, and suggestions for further work of hydrogen embrittlement in high-strength pipeline steels. Int J Hydrog Energy 2022;47(12):8071–90.

[16] Liu ZE, Long W, Chen Z, Littlefield J, Jing L, Ren B, El-Houjeiri HM, Qahtani AS, Jabbar MY, Masnadi MS. A novel optimization framework for natural gas transportation pipeline networks based on deep reinforcement learning. Energy AI 2024;18:100434.

[17] Zhang B, Xu N, Zhang H, Qiu R, Wei X, Wang Z, Liang Y. Influence of hydrogen blending on the operation of natural gas pipeline network considering the compressor power optimization. Appl Energy 2024;358:122594.

[18] Gondal IA. Hydrogen integration in power-to-gas networks. Int J Hydrog Energy 2019;44(3):1803–15.

[19] Topolski K, Reznicek EP, Erdener BC, San Marchi CW, Ronevich JA, Fring L, Simmons K, Fernandez OJG, Hodge B-M, Chung M. Hydrogen blending into natural gas pipeline infrastructure: Review of the state of technology. 2022.

[20] Arsad AZ, Hannan M, Al-Shetwi AQ, Mansur M, Muttaqi K, Dong Z, Blaabjerg F. Hydrogen energy storage integrated hybrid renewable energy systems: A review analysis for future research directions. Int J Hydrog Energy 2022;47(39):17285–312.

[21] Tarhan C, Çil MA. A study on hydrogen, the clean energy of the future: Hydrogen storage methods. J Energy Storage 2021;40:102676.

[22] Saad DM, Sodwatana M, Sherwin ED, Brandt AR. Energy storage in combined gas-electric energy transitions models: The case of california. Appl Energy 2025;385:125480.

[23] A mathematical framework for modelling and evaluating natural gas pipeline networks under hydrogen injection. Int J Hydrog Energy 2008;33(21):6222–31.

[24] Abeysekera M, Wu J, Jenkins N, Rees M. Steady state analysis of gas networks with distributed injection of alternative gas. Appl Energy 2016;164:991–1002.

[25] Adolfo D, Carcasci C, et al. Steady-state simulation of gas distribution networks in the presence of localized hydrogen injections. In: Proceedings of 11th international conference on applied energy, part, vol. 1, 2019, p. 4.

[26] Cheli L, Guzzo G, Adolfo D, Carcasci C. Steady-state analysis of a natural gas distribution network with hydrogen injection to absorb excess renewable electricity. Int J Hydrog Energy 2021;46(50):25562–77.

[27] Kazi SR, Sundar K, Srinivasan S, Zlotnik A. Modeling and optimization of steady flow of natural gas and hydrogen mixtures in pipeline networks. Int J Hydrog Energy 2024;54:14–24.

[28] Timmerberg S, Kaltschmitt M. Hydrogen from renewables: Supply from north africa to central europe as blend in existing pipelines–potentials and costs. Appl Energy 2019;237:795–809.

[29] Pellegrini M, Guzzini A, Saccani C. A preliminary assessment of the potential of low percentage green hydrogen blending in the Italian natural gas network. Energies 2020;13(21):5570.

[30] Erdener BC, Sergi B, Guerra OJ, Chueca AL, Pambour K, Brancucci C, Hodge B-M. A review of technical and regulatory limits for hydrogen blending in natural gas pipelines. Int J Hydrog Energy 2023;48(14):5595–617.

[31] Delaval B, Rapson T, Sharma R, Hugh-Jones W, McClure E, Temminghoff M, Srinivasan V. Hydrogen rd&d collaboration opportunities. 2022.

[32] Pompili B, Maire B. Stratégie nationale pour le développement de l'hydrogène décarboné en France. Tech. rep., 2020, Technical Report. URL: https://minefi hosting. augure. com/Augure_Minefi/r ....

[33] Jin L, Ferrario AM, Cigolotti V, Comodi G. Evaluation of the impact of green hydrogen blending scenarios in the Italian gas network: Optimal design and dynamic simulation of operation strategies. Renew Sustain Energy Transit 2022;2:100022.

[34] Calabrese M, Ademollo A, Busi L, Meazzini M, Carcasci C. Techno-economic assessment of green hydrogen production for blending in the natural gas network. In: Journal of physics: conference series, vol. 2893, (1):IOP Publishing; 2024, 012066.

[35] Clegg S, Mancarella P. Storing renewables in the gas network: modelling of power-to-gas seasonal storage flexibility in low-carbon power systems. IET Gener Transm Distrib 2016;10(3):566–75.

[36] Pedersen J, Hoppmann-Baum K, Zittel J, Koch T. Blending hydrogen into natural gas: An assessment of the capacity of the german gas grid. In: International conference on operations research. Springer; 2021, p. 182–7.

[37] Blunt K. Utilities look to green hydrogen to cut carbon emissions. Wall Str J 2020.

[38] McQueen S, Stanford J, Satyapal S, Miller E, Stetson N, Papageorgopoulos D, Rustagi N, Arjona V, Adams J, Randolph K, et al. Department of energy hydrogen program plan. Tech. rep., US Department of Energy (USDOE), Washington, DC (United States); 2020.

[39] USDepartment of Energy (DoE). Hydrogen shot. 2021.

[40] Galyas AB, Kis L, Tihanyi L, Szunyog I, Vadaszi M, Koncz A. Effect of hydrogen blending on the energy capacity of natural gas transmission networks. Int J Hydrog Energy 2023;48(39):14795–807.

[41] EIA. Natural gas processing plant survey. 2017, https://atlas.eia.gov/datasets.

[42] HIFLD. Power plants. 2022, https://hifld-geoplatform.hub.arcgis.com/datasets/geoplatform::power-plants-2/about.

[43] Chen Z, Zhong R, Long W, Tang H, Wang A, Liu Z, Yang X, Ren B, Littlefield J, Koyejo S, et al. Advancing oil and gas emissions assessment through large language model data extraction. Energy AI 2025;20:100481.

[44] NREL. Innovative data energy applications. 2015, https://maps.nrel.gov/?da=hydra.

[45] Liu ZE, Moya D, Chen Z, Long W, Jing L, Ren B, Tang H, Jabbar MY, Ramadan F, Littlefield J, Masnadi MS. Algorithm for transportation pathways and patterns through pipeline network: A case study in california for the power generation sector. Engineering 2025. http://dx.doi.org/10.1016/j.eng.2025.11.005.

[46] Ulvestad M, Overland I. Natural gas and CO2 price variation: impact on the relative cost-efficiency of LNG and pipelines. Int J Environ Studies 2012;69(3):407–26.

[47] Greene S, Jia H, Rubio-Domingo G. Well-to-tank carbon emissions from crude oil maritime transportation. Transp Res Part D: Transp Environ 2020;88:102587.

[48] Zubair M, Chen S, Ma Y, Hu X. A systematic review on carbon dioxide (CO2) emission measurement methods under PRISMA guidelines: transportation sustainability and development programs. Sustainability 2023;15(6):4817.

[49] Winarno E, Hadikurniawati W, Rosso RN. Location based service for presence system using haversine method. In: 2017 international conference on innovative and creative information technology (iCITech). IEEE; 2017, p. 1–4.

[50] Wang G, Cheng Q, Zhao W, Liao Q, Zhang H. Review on the transport capacity management of oil and gas pipeline network: Challenges and opportunities of future pipeline transport. Energy Strat Rev 2022;43:100933.

[51] Farag HE, Al-Obaidi A, Khani H, El-Taweel N, El-Saadany E, Zeineldin H. Optimal operation management of distributed and centralized electrolysis-based hydrogen generation and storage systems. Electr Power Syst Res 2020;187:106476.

[52] Kim J, Chun KM, Song S, Baek H-K, Lee SW. Hydrogen effects on the combustion stability, performance and emissions of a turbo gasoline direct injection engine in various air/fuel ratios. Appl Energy 2018;228:1353–61.

[53] Zhao Y, McDonell V, Samuelsen S. Influence of hydrogen addition to pipeline natural gas on the combustion performance of a cooktop burner. Int J Hydrog Energy 2019;44(23):12239–53.

[54] Liu ZE, Zhou Q, Li Y, Shuai S, Xu H. Safe deep reinforcement learning-based constrained optimal control scheme for HEV energy management. IEEE Trans Transp Electrification 2023;9(3):4278–93. http://dx.doi.org/10.1109/TTE.2023.3240430.

[55] Liu ZE, Li Y, Zhou Q, Shuai B, Hua M, Xu H, Xu L, Tan G, Li Y. Real-time energy management for HEV combining naturalistic driving data and deep reinforcement learning with high generalization. Appl Energy 2025;377:124350.

[56] Haeseldonckx D, D'haeseleer W. The use of the natural-gas pipeline infrastructure for hydrogen transport in a changing market structure. Int J Hydrog Energy 2007;32(10–11):1381–6.
[57] Altfeld K, Pinchbeck D. Admissible hydrogen concentrations in natural gas systems. Gas Energy 2013;2103(03):1–2.
[58] Zhou D, Yan S, Huang D, Shao T, Xiao W, Hao J, Wang C, Yu T. Modeling and simulation of the hydrogen blended gas-electricity integrated energy system and influence analysis of hydrogen blending modes. Energy 2022;239:121629.
[59] Kazi SR, Sundar K, Zlotnik A. Dynamic optimization and optimal control of hydrogen blending operations in natural gas networks. In: 2024 American control conference. ACC, IEEE; 2024, p. 5357–63.
[60] Von Wald GA, Stanion AJ, Rajagopal D, Brandt AR. Biomethane addition to california transmission pipelines: Regional simulation of the impact of regulations. Appl Energy 2019;250:292–301.
[61] Rosa N, Fereidani NA, Cardoso BJ, Martinho N, Gaspar A, da Silva MG. Advances in hydrogen blending and injection in natural gas networks: A review. Int J Hydrog Energy 2025;105:367–81.